ENHANCING THE FLEXURAL BEHAVIOUR OF SUSTAINABLE FERROCEMENT-RETROFITTED RC BEAMS: IMPACT OF WASTE BRICK POWDER AND GI WIRE FIBRES

Md Jihad Miah[1*], Mohammad Shamim Miah[2], Humera Mughal[3], Md Kawsar Ali[4], Md. Munir Hossain Patoary[5]

[1] *Lecturer, Civil Engineering, School of Architecture, Technology and Engineering, University of Brighton, Lewes Road, Brighton BN2 4GJ, England, UK, e-mail: M.J.Miah@brighton.ac.uk*
[2] *Senior Researchers, Institute of Engineering Geodesy and Measurement Systems, Graz University of Technology, 8010 Graz, Austria, e-mail: miah@tugraz.at*
[3] *Assistant Professor, College of Architecture and Design, Prince Sultan University, Salman Neighborhood, Riyadh 12435, Saudi Arabia, e-mail: hmughal@psu.edu.sa*
[4] *Materials Engineer, Abdul Monem Limited, Dhaka-1205, Bangladesh, e-mail: kawsar.uap@gmail.com*
[5] *PhD Student, Department of Civil Engineering, Bangladesh University of Engineering and Technology, Dhaka-1000, Bangladesh, e-mail: 3dcometdesign@gmail.com & 0422044016@ce.buet.ac.bd*

***Corresponding Author**

ABSTRACT

Ferrocement is a composite material made from cement mortar and steel mesh. It is known for its high tensile strength, resistance to cracking, and durability. These qualities make it a good choice for repairing damaged concrete. However, weak bonding between the mortar, mesh, and existing concrete can lead to brittleness, reduced ductility, and interfacial separation. To address the research gap, this study evaluated four reinforced concrete (RC) beams that were damaged and subsequently repaired using ferrocement. Their performance was compared with that of an unretrofitted beam (URB). In the study, sand (S) was partially replaced with waste brick powder (WBP), and 3% low-cost galvanised iron wire fibres (GIF) were incorporated to produce a ductile mortar. The four RC beams were retrofitted with ferrocement mortar in the following configurations: (i) 100% S, (ii) 50% WBP + 50% S (50-50 WBP-S), (iii) 100% S + 3% GIF, and (iv) 50-50 WBP-S + 3% GIF. Furthermore, a data-driven mathematical model was developed, verified, and optimised based on the experimental results. The outcomes indicate that the ferrocement-retrofitted RC beam with 100% S achieved a 3% improvement in flexural load compared to the URB. In contrast, the beam retrofitted with 50% WBP as a replacement for sand (50-50 WBP-S) demonstrated a significant enhancement, achieving a 19% higher flexural load than the URB. Notably, both the damaged beams retrofitted with 100% S and 50-50 WBP-S incorporating 3% GIF showed substantial increases in flexural load, with gains of 42% for 100% S + 3% GIF and 58% for 50-50 WBP-S + 3% GIF when compared to the URB. The deflection increased by 141% for the 100% S + 3% GIF beam and by 203% for the 50-50 WBP-S + 3% GIF beam compared to the URB. The data-based model accurately reflects the load-deflection profile, achieving a coefficient of determination (R^2) of 0.9580-0.9974, thereby validating its effectiveness—even in the presence of both minor and major cracks. Conversely, the optimised model demonstrates strong agreement with the experimental results, closely matching the observed data throughout the entire profile.

Keywords: *Waste brick powder, GI wire fibre, ferrocement-retrofitting, flexural performance, data-driven model*

1. INTRODUCTION

Cementitious composites, especially concrete, are widely used in construction due to their high compressive strength, cost-effectiveness, and durability (Domone & Illston, 2010; Mehta & Monteiro, 2006). However, concrete's brittleness and low tensile strength make structures susceptible to damage from environmental factors, seismic events, fire, and increased loads (Miah et al., 2022a; Miah et al., 2022b; Miah et al., 2023). Design flaws, material fatigue, and complex loading can lead to cracking, compromising the structural integrity of reinforced concrete (RC) beams. Therefore, strategically retrofitting ageing RC members is essential to ensure safety, extend lifespan, and meet modern load requirements, thus avoiding the need for demolition (Huang et al., 2022; Miah et al., 2025). This rehabilitation reduces the risk of failure and lifecycle costs while promoting sustainability by minimising resource use and waste. Retrofitting interventions are vital for maintaining the reliability of critical infrastructure.

There are many techniques to rehabilitate concrete structures by improving their strength, ductility, and durability. Common methods include jacketing (Fathalla & Mihaylov, 2025), CFRP wrapping (Liu et al., 2025), UHPC overlays (Huang et al., 2022), carbonation curing (Liu et al., 2023), and diammonium hydrogen phosphate treatment (Miah et al., 2024). Among these, ferrocement composites—composed of cement mortar reinforced with layered steel mesh—are particularly notable for their favourable mechanical properties, cost-effectiveness, and ease of application with local materials (Miah et al., 2025a; Miah et al., 2025b). This makes them especially valuable for projects in developing countries. Ferrocement acts as an external shell, enhancing tensile capacity and seismic resilience. However, there are some drawbacks; the steel mesh can be susceptible to corrosion in harsh environments, and high-strength mortars may lead to shrinkage cracking and reduced ductility. Therefore, to maximise the effectiveness of ferrocement, careful selection of materials and precise application techniques are essential.

The conventional formulation of ferrocement primarily uses natural sand as its fine aggregate, sourced mainly from riverbeds. This reliance on a finite resource leads to environmental challenges, including riverbank erosion and habitat destruction, driven by intensive sand mining associated with urbanisation (Miah et al., 2021). In some regions, particularly in Asia, where natural stone is limited, clay bricks have become a viable alternative aggregate (Miah et al., 2022a; Miah et al., 2022b). This process generates a fine fraction often regarded as waste, leading to underutilisation in structural applications due to a lack of comparative performance data. Research indicates that waste brick powder (WBP) particles form stronger bonds at the aggregate-cement interface, thereby enhancing the mechanical properties and durability of the composite. Notably, a mortar mix with 50% replacement of natural sand showed a 25% increase in compressive strength, a 31% increase in tensile strength, and a 31% increase in flexural strength (Miah et al., 2021). The utilisation of WBP in ferrocement retrofitting would not only mitigate the environmental impact of sand mining but also promote sustainable construction by repurposing industrial byproducts into valuable applications.

The integration of advanced computational methods has revolutionised concrete design by allowing for highly accurate virtual modelling of structural behaviour. Techniques such as finite element analysis, machine learning algorithms, and data-driven modelling are now employed to predict key performance metrics, including load-bearing capacity, deflection characteristics, and potential failure modes (Miah et al., 2025a; Miah et al., 2025b). These predictions are based on input variables such as material composition and boundary conditions. This shift toward simulation-driven design significantly reduces reliance on iterative physical prototyping, leading to improved resource allocation efficiency, cost savings, and shorter project timelines. By accurately forecasting the mechanical properties and performance of structures, these advanced analytical tools are vital for developing environmentally friendly and cost-effective concrete formulations.

While the ferrocement retrofitting techniques discussed earlier have been studied, the issues related to the brittleness of cement mortar and the weak bond between the steel mesh, the parent concrete, and the mortar have not been thoroughly investigated. Moreover, the use of waste brick powder (WBP) as a sand substitute in ferrocement mortar is not well explored in the literature. Additionally, there is a lack of information regarding load-deflection predictions for sustainable ferrocement-retrofitted RC beams made with WBP and fibres using data-driven models. This research aims to fill a critical

knowledge gap by evaluating the structural performance of RC beams retrofitted with a new ferrocement system utilising sustainable, ductile mortar mixes. In this experimental investigation, four damaged RC beams were rehabilitated with ferrocement overlays, and their performance was compared with that of an unretrofitted beam (URB). The study employed a modified, ductile mortar formulation, where a portion of the 50% natural sand was replaced with WBP, and the mix was enhanced with 3% by volume of galvanised iron wire fibres (GIF). The four retrofitted beams were designed to assess different mortar compositions: a conventional 100% sand mix (100% S), a 50% WBP and 50% sand blend (50-50 WBP-S), a fibre-reinforced mix with 100% sand and 3% GIF (100% S + 3% GIF), and a hybrid mix consisting of both 50% WBP and 50% sand along with 3% GIF (50-50 WBP-S + 3% GIF). In addition to the experimental program, a data-driven mathematical model was developed, verified, and then the models were optimised to fit the experimental results closely.

2. EXPERIMENTAL METHODOLOGY

The experimental program involved casting five reinforced concrete (RC) beams measuring 750 mm by 125 mm by 200 mm for flexural testing. All specimens were designed with a consistent concrete clear cover of 20 mm. One beam was designated as an unretrofitted beam (URB), while the other four were designated for retrofitting. The detailed reinforcement specifications for the RC beams are illustrated in Figure 1. All RC beams were made with a water-cement ratio of 0.55 and a cement (CEM II 42.5 N) content of 350 kg/m³. The mixture consisted of 772 kg/m³ of brick coarse aggregate, 829 kg/m³ of sand, and 193 kg/m³ of water, and it was produced without any chemical admixtures. After a standard 28-day water-curing period, all beams underwent four-point bending tests on a load-controlled universal testing machine. Each beam was loaded until nearing total failure before any retrofitting was applied. The control URB beam was continuously loaded until it collapsed structurally. Beam deflection was monitored using three linear variable-displacement transducers (LVDTs), as shown in Figure 1. The resulting failure load for the URB beam was recorded at 143 kN. Major flexural and diagonal cracking was observed to occur at a load of approximately 120 kN.

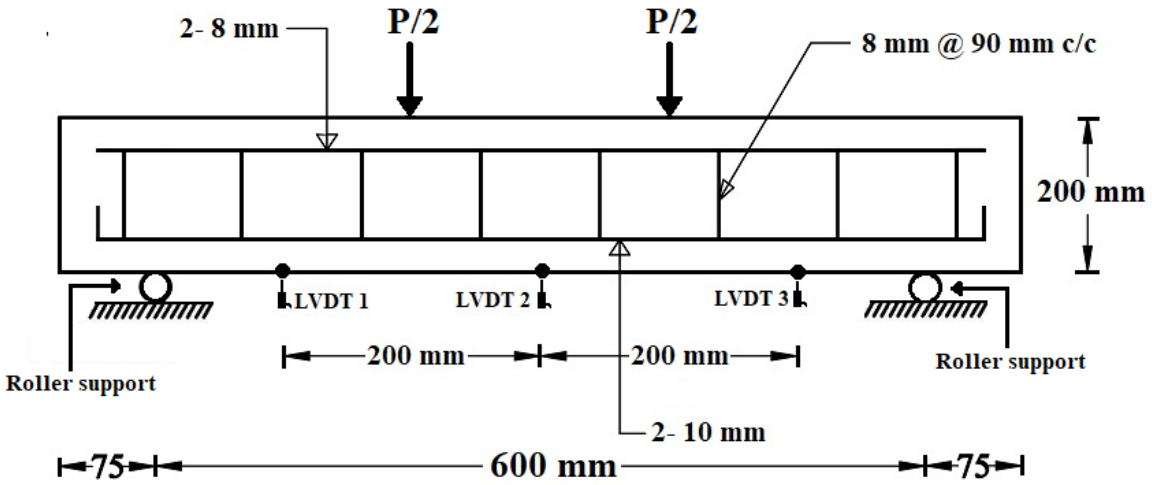

Figure 1: Reinforcement details of the RC beams and flexural test setup with LVDTs.

For the ferrocement retrofit, a controlled load of 130 kN was applied, which is approximately 91% of the average failure load of 143 kN observed in the URB. This load was intentionally selected to induce significant damage, as major flexural and diagonal cracking began at about 120 kN. After unloading, the beam surfaces were prepared for retrofitting. This involved roughening the substrate with metal hammers and cleaning it with a wire brush to remove debris without causing additional damage. A U-shaped steel wire-mesh jacket was then secured to the three sides of the beams using stainless steel fasteners, as illustrated in Figure 2. Finally, a ductile, fibre-reinforced cement mortar was applied in a 10-15 mm layer to encapsulate the mesh and restore the beam's profile, ensuring

optimal bonding with the original substrate (see Figure 2). The novel ductile mortar was developed in which 50% of the sand volume was replaced with WBP. This WBP is a byproduct created from processing demolition waste—specifically, aged bricks salvaged from old masonry structures—into coarse aggregate. The resulting brick powder was sieved to ensure all particles were finer than 4.75 mm, classifying it as a fine aggregate. Figure 3 illustrates the sand and WBP. The grain-size distributions of the sand and WBP are illustrated in Figure 4, where WBP follows a trend similar to that of sand. As illustrated in Figure 3, the mechanically crushed WBP particles are more angular and exhibit a rougher texture. In contrast, the river sand grains are typically smoother and more rounded. To create the sustainable, ductile ferrocement mortar, inexpensive, locally sourced galvanised iron (GI) wire was cut into fibres. Each fibre was made to a length of 13 mm with a diameter of 0.70 mm, as shown in Figure 3. The ductile ferrocement mortar formulations were prepared by adding 3% mortar by volume. The binder for the ferrocement mortar remained CEM II 42.5 N cement. CEM II 42.5 N composition mainly consists of clinker (80–94%), which is partially replaced by 6–20% of various supplementary cementitious materials, including industrial by-products such as fly ash and granulated slag. Additionally, a small amount of gypsum (≤5%) is included as a set-controlling additive.

Figure 2: Damaged RC beam and preparation of ferrocement-retrofitting RC beams.

Figure 3: Image of sand (S), waste brick powder (WBP), and galvanised iron wire fibres (GIF).

Four mortar formulations were developed for the ferrocement overlays, using a water-cement ratio of 0.30. The mixes are as follows: a conventional mix consisting of 100% sand (100% S), a blend of 50% WBP and 50% sand (50-50 WBP-S), a fibre-reinforced mix containing 100% sand and 3% GIF (100% S + 3% GIF), and a hybrid mix that combines 50% WBP and 50% sand with 3% GIF (50-50 WBP-S + 3% GIF). The mortar mix designs are summarised in Table 1. Following the 28-day water-curing period, the retrofitted beams were subjected to four-point bending tests until failure. Their deflection was monitored throughout using three LVDTs, whose positions are illustrated in Figure 1.

Table 1: Mix design of sustainable ferrocement mortar mixes.

Mix ID	Cement (kg/m^3)	Sand (kg/m^3)	WBP (kg/m^3)	Water (kg/m^3)	GIF (%)
100% S	640	1280	-	192	0
50-50 WBP-S	640	640	494	192	0
100% S + 3% GIF	640	1280	-	192	3
50-50 WBP-S + 3% GIF	640	640	494	192	3

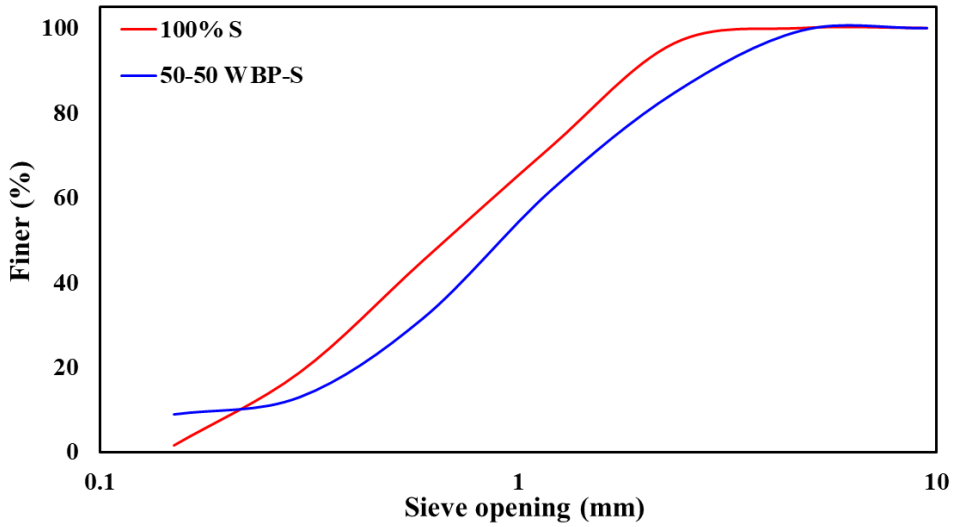

Figure 4: Gradation curves of sand and WBP.

3. DATA-DRIVEN MODELLING AND OPTIMISATION

In most cases, performing experimental tests is not feasible. Hence, having a data-based model might be useful for evaluating different possible outcomes. The data-driven models are not only useful for rendering current behaviour but can also be used to predict (Fan, 1996). Selecting a model type can be challenging due to the numerous options, including linear, nonlinear, physics-based, and non-physics-based models (Fan, 1996; Miah & Lienhart, 2023). Herein, the regression-type model has been selected due to their straightforward structure but robust performance (Miah et al., 2018). For the study, a generic expression for the model under study is as follows.

$$F = f(\delta, \theta) + \varepsilon \tag{1}$$

where F represents the model output, δ is the independent variable, θ represents the unknown coefficients of the model, and ε is the error term. Further, the above equation can be described by,

$$F = \theta_1\delta^4 + \theta_2\delta^3 + \theta_3\delta^2 + \theta_4\delta + \theta_5 \tag{2}$$

where F is the flexural load, δ is the deflection, $\theta_1, \theta_2, \theta_3, \theta_4$, and θ_5 are the coefficients of the model. By using the coefficient values, the above equation can be expressed as,

$$F = -0.23\delta^4 + 5.16\delta^3 - 40\delta^2 + 130.60\delta + 18.89 \quad (3)$$

After developing the model, the designer may proceed to optimise performance further. Optimisation can be achieved using various optimisation algorithms, such as linear, nonlinear, constrained, unconstrained, heuristic, or search-based (Miah & Lienhart, 2023; Lagarias et al., 1998). However, to find a global minimum rather than a local minimum, a heuristic optimisation algorithm has been adopted due to its superior performance (Lagarias et al., 1998; Miah, 2020). By employing the early-mentioned optimisation techniques, the following objective function (J) needs to be optimised.

$$J = \sqrt{\sum_{i=1}^{N} \frac{|f^{true} - f^{model}|^2}{|f^{true}|^2}} \quad (4)$$

where f^{true} is the experimental data, f^{model} is the developed model's outcome.

4. EXPERIMENTAL OUTCOMES AND DISCUSSIONS

Figure 5 illustrates the mid-span load-deflection behaviour of all the retrofitted beams. For comparison, the response of the unretrofitted beam (URB) is also included. The results indicate that the ferrocement overlay significantly improved flexural performance, even without fibre inclusion. Beams using 100% S mortar achieved an average failure load of 147 kN, representing a 3% increase over the URB's 143 kN capacity, as reported in Figure 6. The significant increase in flexural load capacity of ferrocement retrofitted RC beams is attributed to the synergistic effects between the retrofitted layer and the original beam. The ferrocement layer, free of coarse aggregates, allows a high reinforcement density within a thin profile, enhancing strength without adding substantial weight. This system relies on composite action, where a tightly packed steel wire mesh ensures uniform stress distribution, minimising localised cracking and improving tensile resistance (Miah et al., 2025a; Miah et al., 2025b).

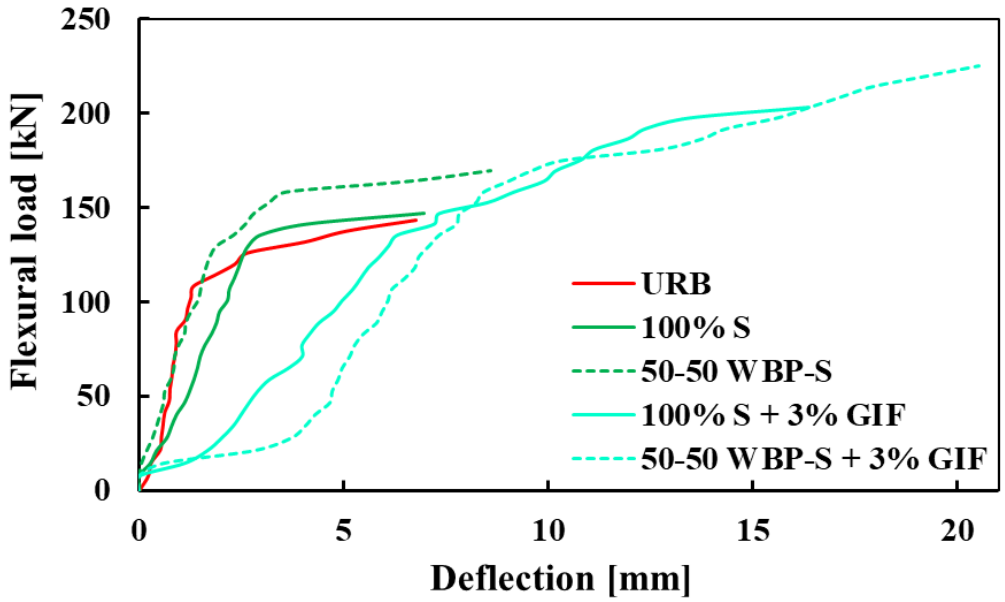

Figure 5: Load-deflection of the URB and ferrocement-retrofitted RC beams measured at their midpoints, fabricated with different mortar compositions: 100% S, 50-50 WBP-S, 100% S + 3% GIF, and 50-50 WBP-S + 3% GIF.

This effectively delays crack initiation and promotes ductile failure. The high-performance mortar matrix, containing 640 kg/m³ of cement with a water-to-cement ratio of 0.30, serves two purposes: it repairs microcracks and creates a low-porosity, impermeable barrier. This is accomplished through a microfiller effect from supplementary cementitious materials (SCMs) used with CEM II cement, which blocks pores and enhances the interfacial transition zone (ITZ) through pozzolanic reactions and ongoing autogenous healing. The substrate process of chipping beam surfaces results in roughened surfaces, which ensure a strong bond at the interface between the mortar, wire mesh, and parent concrete.

Furthermore, the use of 50% WBP as sand replacement in a blend mix (50-50 WBP-S) further enhanced performance, resulting in a failure load of 170 kN, approximately a 19% increase compared to the URB, as reported in Figure 6. This enhancement is attributed to the unique particle characteristics of WBP. Mechanically crushed WBP exhibits an angular, rough morphology (see Figure 3), which promotes better mechanical interlocking with the cement paste than smoother, rounded sand particles. Additionally, the particle size distribution of WBP (see Figure 4) shows a significantly higher proportion of fine particles (less than 0.15 mm) — approximately 2.1 times more than sand. These fine particles effectively fill capillary pores, reducing permeability and strengthening the ITZ (Miah et al., 2025a; Miah et al., 2025b; Huang et al., 2021). Furthermore, the increased fineness enhances WBP's pozzolanic potential (Huang et al., 2021; Miah et al., 2021). The larger surface area of these particles accelerates the chemical reactions between the silica and alumina in WBP and the calcium hydroxide formed during cement hydration, leading to the production of additional strength-giving calcium silicate hydrate (C-S-H) gel (Miah et al., 2025a; Miah et al., 2025b; Huang et al., 2021). This process contributes to a denser microstructure, as corroborated by Huang et al. (2021). The combined effect of this optimised mortar matrix and the high-strength, texturally advantageous steel mesh (see Figure 3) creates a system that significantly improves crack resistance and load redistribution, thereby explaining the superior flexural performance compared to the URB.

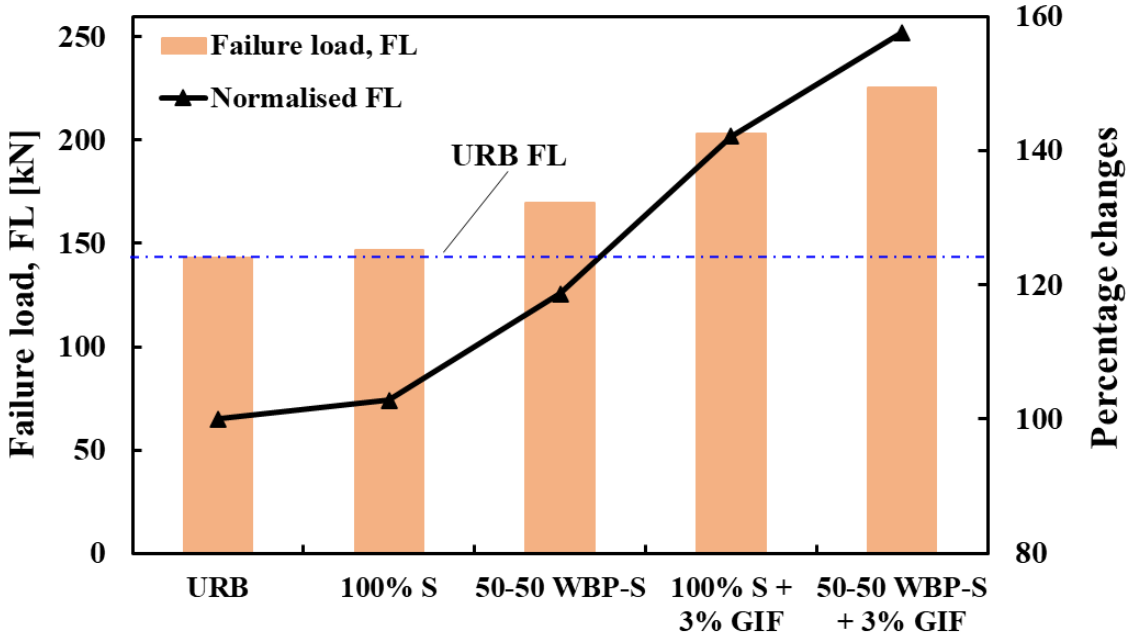

Figure 6: Failure load of the URB and ferrocement-retrofitted RC beams prepared with different mortar compositions: 100% S, 50-50 WBP-S, 100% S + 3% GIF, and 50-50 WBP-S + 3% GIF.

The flexural performance of RC beams significantly improves with the addition of GIF to ferrocement mortar. Experimental results indicate that beams containing 3% GIF achieved failure loads of 203.30 kN for the ferrocement mortar mix with 100% S + 3% GIF, and 225.40 kN for the mix with 50-50 WBP-S + 3% GIF. When compared to the URB, the flexural load increased by 42% for the mortar mix with 100% S + 3% GIF, and by 58% for the mix with 50-50 WBP-S + 3% GIF. Additionally,

when comparing these results to ferrocement RC beams made solely with 100% S and 50-50 WBP-S, the enhancements were 38.3% for the mix with 100% S + 3% GIF, and 32.8% for the mix with 50-50 WBP-S + 3% GIF. The improvement in flexural strength of beams containing GIF arises from both structural and material-level contributions. In conventional cement-based beams without fibre reinforcement, the stress distribution during bending is characterised by compressive stresses at the top and tensile stresses at the bottom (Miah et al., 2025a; Miah et al., 2025b). While cement mortars can withstand high compressive loads, their tensile resistance is limited, making them vulnerable to brittle fracture when bent. This often leads to early cracking on the tension side, which can propagate rapidly through existing voids and weak spots in the matrix. This eventually causes debonding at the interfaces of the mortar, steel mesh, and concrete, leading to sudden failure under relatively small loads (Miah et al., 2025a; Miah et al., 2025b). In contrast, incorporating GIFs into the mortar significantly changes this behaviour. The fibres provide a bridging action across developing cracks, absorbing tensile forces once the cement matrix has cracked and redistributing stresses in the fracture region. The fibres also limit crack widening and delay growth, improving ductility, post-cracking load capacity, and resistance to shrinkage-induced cracking (Miah et al., 2025b). However, the effectiveness of this reinforcement is strongly influenced by the orientation and dispersion of the fibres within the mix. A mostly uniform, random, but horizontal fibre alignment—observed in the prepared beams—enabled better stress transfer and crack control, while unfavourable alignment or clustering can reduce the reinforcement effect. Cementitious composites are inherently prone to shrinkage as they dry and undergo chemical transformations during hydration, generating internal tensile stresses that weaken the material in the absence of fibres. In mixes without GIF reinforcement, this shrinkage-induced stress often leads to cracking, compromising the mortar's overall mechanical reliability. However, the inclusion of GIFs mitigates this issue by inhibiting crack formation in the early stages, thereby allowing the mortar to accommodate volume changes better. Consequently, the fibres not only reduce shrinkage-related damage but also enhance the composite's strength and durability. As a result, fibres can withstand greater stress, improve energy absorption, and contribute to a more gradual failure process than fibre-free beams.

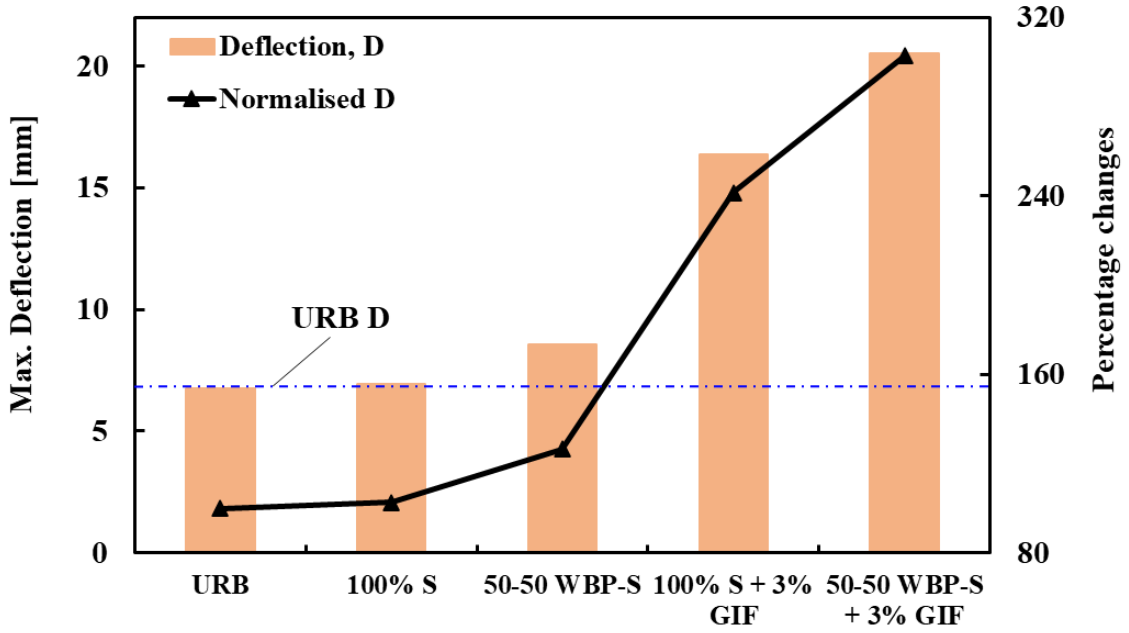

Figure 7: Maximum deflection of the URB and ferrocement-retrofitted RC beams cast with different mortar compositions: 100% S, 50-50 WBP-S, 100% S + 3% GIF, and 50-50 WBP-S + 3% GIF.

Figure 7 presents the maximum mid-span deflection values recorded across the tested beams. When strengthened with ferrocement but without GIF, the beams already showed enhanced deformability, with the 100% S and 50–50 WBP-S mixes achieving deflection increases of about 3% and 27% relative to the URB, respectively. Introducing 3% GIF into the ferrocement mortar significantly improved the mid-span deflection of the RC beams, with values of 141% for 100% S + 3% GIF and

203% for 50-50 WBP-S + 3% GIF, both higher than the URB. These enhancements are approximately 135.4% for 100% S + 3% GIF and 139.1% for 50-50 WBP-S + 3% GIF, which is higher than those of the beams with 100% S and 50–50 WBP-S.

The enhanced mid-span deflection observed in beams reinforced with GIF can be attributed to their improved tensile resistance. The fibres act as bridges across cracks, distributing stresses more evenly between the mortar and the fibre network. When comparing beams made with only 100% S to those fabricated with a 50-50 WBP-S mix, the latter demonstrated even greater deformability, highlighting the impact of the matrix composition. The superior performance of these beams can be attributed to several factors, including fibre bridging, strong interfacial bonds between the concrete, ferrocement mesh, fibres, and mortar. Consequently, GIF-reinforced beams can sustain elongation under high loads, enabling greater plastic deflection, effective load redistribution, and improved energy absorption. In contrast to URB, which often fails abruptly, these reinforced specimens exhibited gradual, ductile failure. This behaviour is particularly advantageous in structural applications because it enhances safety margins and provides critical warning signs before a collapse, giving occupants valuable time to evacuate during extreme events such as earthquakes, blasts, or tsunamis.

5. DATA-DRIVEN MODEL OUTCOMES AND DISCUSSIONS

For the numerical study, all 5 RC beams were examined, both without and with ferrocement mortar, as well as with GIF. The load-deflection responses of the RC beams obtained from these experiments were simulated using a data-driven model, and the model's outcomes are illustrated in Figure 8. The comparison demonstrated strong agreement between the simulated and experimental curves, which achieved a coefficient of determination (R^2) of 0.9580, 0.9974, 0.9927, 0.9941, and 0.9836, for the URB and ferrocement RC beams retrofitted with the mortar mixes 100% S, 50-50 WBP-S, 100% S + 3% GIF and 50-50 WBP-S + 3% GIF, respectively. The models accurately captured the initial linear elastic behaviour up to approximately 100-130 kN, depending on the beams, where deflection increased proportionally with the load. Beyond this point, concrete cracking introduced nonlinear behaviour, followed by reinforcement yielding and crack propagation, leading to failure. The models reproduced this transition with reasonable accuracy; some discrepancies were observed in the post-cracking regime due to its highly nonlinear nature.

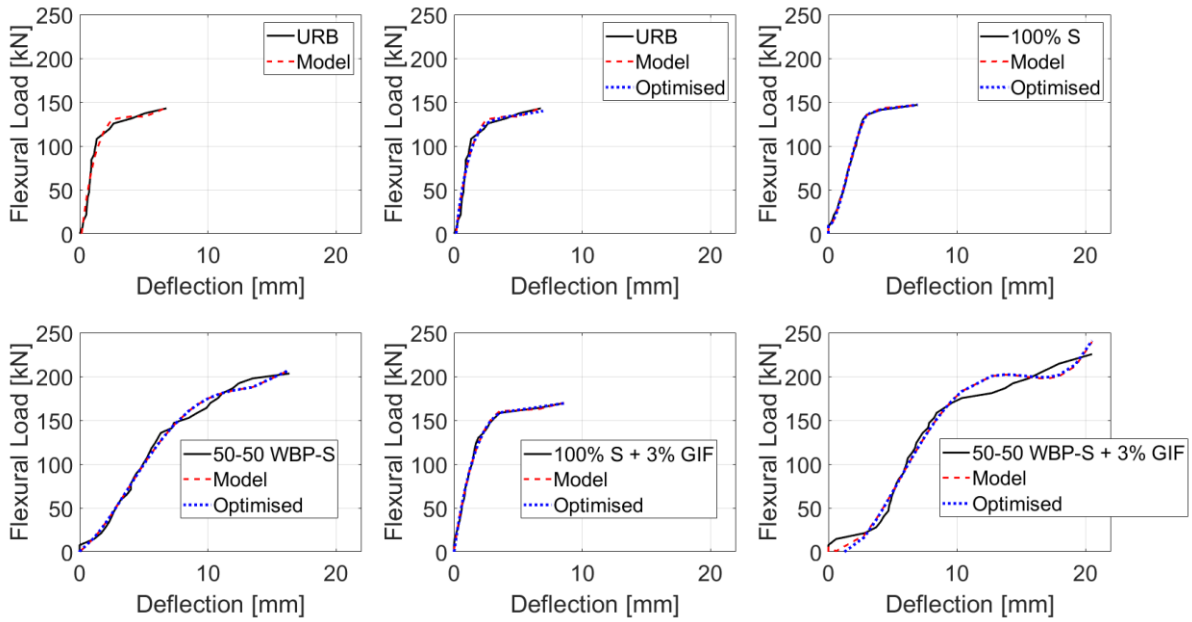

Figure 8: Predicted load-deflection and optimised outcomes of the URB and ferrocement-retrofitted RC beams cast with different mortar compositions: 100% S, 50-50 WBP-S, 100% S + 3% GIF, and 50-50 WBP-S + 3% GIF.

To enhance predictive capacity, optimisation procedures were applied to the model, named Optimised, as shown in Figure 8. As shown in the Figure, optimisation only slightly improved performance, as the baseline model had already produced highly reliable results. This aligns with previous findings reported by Miah et al., 2025a and Miah et al., 2025b, which suggested that optimisation is most beneficial when initial models significantly deviate from experimental trends. In this study, given the already strong predictive correlation ($R^2 > 0.95$), further optimisation for beams strengthened with ferrocement and GIF with sand and WBP was deemed unnecessary. Extending the optimisation would have added computational costs, increased complexity, and prolonged development time without yielding meaningful improvements. Consequently, the baseline models were retained, striking a balance between predictive accuracy and practical efficiency for the analysis of ferrocement-strengthened RC beams.

6. CONCLUSIONS

This study investigates the impact of using 50% WBP as a sand replacement and incorporating 3% GIF on the flexural behaviour of RC beams that have been retrofitted with ferrocement mortar. The performance of these beams is compared with that of a URB beam and a ferrocement-retrofitted beam made with 100% sand. The load-deflection characteristics of the beams were examined, and their behaviour was further analysed using a data-driven model, which was subsequently optimised to align closely with the experimental results. The testing program revealed that applying ferrocement mortar to RC beams, even in the absence of GIF reinforcement, significantly increased their flexural strength compared to the URB. Specifically, there were strength increases of about 3% for the RC beams with ferrocement mortar containing 100% S and 19% for the 50-50 WBP-S mixture. The introduction of GIF into the ferrocement mortar markedly enhanced the flexural performance. Strength improvements were recorded at 42% for the ferrocement beams with 100% S + 3% GIF, and 58% for the 50-50 WBP-S + 3% GIF. In terms of deflection, both the beams without GIF and those reinforced with GIF exhibited significantly higher deformation capacities compared to the URB. The deflection increases were 3%, 27%, 141%, and 203% for the ferrocement beams with 100% S, 50-50 WBP-S, 100% S + 3% GIF, and 50-50 WBP-S + 3% GIF, respectively. Overall, the inclusion of GIFs improved plasticity, stress redistribution, and energy absorption, thereby promoting a more ductile failure mode. This is beneficial for structural safety, as it provides valuable warning signs before collapse. Numerical modelling supported these findings by accurately reproducing the experimental load-deflection behaviour during both pre- and post-cracking stages. The models achieved consistently high coefficients of determination ($R^2 > 0.95$), confirming their reliability. After optimisation, the models demonstrated even closer alignment with experimental data across the entire loading range.

ACKNOWLEDGEMENTS

The authors acknowledge the facilities provided by the Department of Civil Engineering at the University of Asia Pacific for this research. Thanks to M.R. Hoque, M.A. Miah, and R.A. Raj for participating in this research project as part of their undergraduate thesis.

DECLARATION OF USE OF AI

The authors declare that no artificial intelligence (AI) tools were used in the preparation of this manuscript. Grammarly software was used solely to improve language style, grammar, and clarity. The software did not contribute to the study design, data analysis, interpretation of results, or generation of scientific content.

REFERENCES

Domone, P., and Illston, J. (2010). Construction Materials: Their Nature and Behaviour. 4th ed.; Spon Press 270 Madison Avenue: New York, NY, USA.

Fan, J. (1996). Local Polynomial Modelling and Its Applications: From linear regression to nonlinear regression. Monographs on Statistics and Applied Probability. Chapman & Hall/CRC. ISBN 978-0-412-98321-4.

Fathalla, E., Mihaylov, B. (2025). Shear behaviour of deep beams strengthened with high-strength fiber reinforced concrete jackets. *Engineering Structures*, 325 (2025) 119404.

Huang, Y., Grünewald, S., Schlangen, E., Lukovic, M. (2022). Strengthening of concrete structures with ultra high performance fiber reinforced concrete (UHPFRC): A critical review. *Construction and Building Materials*, 336: 127398.

Huang, Q., Zhu, X., Xiong, G., Wang, C., Liu, D., Zhao, L. (2021). Recycling of crushed waste clay brick as aggregates in cement mortars: An approach from macro- and micro-scale investigation. *Construction and Building Materials*, 274: 122068.

Liu, J., Fan, X., Zou, L., Shi, C. (2025). Effect of different CFRP strengthening methods on fracture parameters of concrete beam. *Engineering Fracture Mechanics*, 314: 110748.

Liu, T., Wang, H., Zou, D., Long, X., Miah, M.J., Li, Y. (2023). Strength recovery of thermally damaged high-performance concrete subjected to post-fire carbonation curing. *Cement and Concrete Composites,* 143: 105273.

Lagarias JC, Reeds JA, Wright MH, Wright PE. (1998). Convergence Properties of the Nelder-Mead Simplex Method in Low Dimensions. *SIAM Journal on Optimisation*, 9(1): 112–47.

Mehta, P.K., and Monteiro, P.J.M. (2006). Concrete microstructure, properties and materials. McGraw-Hill, New York, NY, USA.

Miah, M.J., Babafemi, A.J., Li, Y., Kong, S.Y., Paul, S.C., Jang, J.G. (2022a). Impact of overburnt distorted brick aggregate on the performance of concrete at ambient temperature and after exposure to elevated temperatures. *Construction and Building Materials* 349: 128792.

Miah, M.J., Babafemi, A.J., Paul, S.C., Kong, S.Y., Li, Y., Jang, J.G. (2022b). Eco-friendly concrete with chemically treated end-of-life tires: mechanical strength, shrinkage, and flexural performance of RC beams. *Construction and Building Materials,* 351:128970.

Miah, M.J., Lo Monte, F., Felicetti, R., Pimienta, P., Carré, H., La Borderie, C. (2023). Impact of external biaxial compressive loading on the fire spalling behavior of normal-strength concrete. *Construction and Building Materials,* 366: 130264.

Miah, M.J., Miah, M.S., Hasan, N.M.S., Sobuz, M.H.R., & Li, Y. (2025a). Role of recycled crushed clay bricks as fine aggregates in enhancing the performance of ferrocement-strengthened RC beams. *Construction and Building Materials,* 478: 141412.

Miah, M.J., Thygesen, J., Simonsen, M.E., Nielsen, R.P., Wu, M. (2024). Strengthening the bulk properties of cement mortar through promoted in-situ formation of hydroxyapatite: Feasibility and perspectives. *Construction and Building Materials,* 459: 139773.

Miah, M., Miah, M.S. (2025b). Sustainable strengthening of RC beams using ferrocement with recycled clay bricks: Role of areca nut husk and jute fibres. *Structures*, 80:109819.

Miah, M.J., Sagar, S.U., Paul, S.C., Babafemi, A.J. (2021). Feasibility of using recycled burnt clay brick waste in cement-based mortar: Mechanical properties, durability, and residual strength after exposure to elevated temperatures. *International Journal of Civil Engineering,* 19:1055–1069.

Miah, M.S., Lienhart, W. (2023). Data-Based Prognosis and Monitoring of Civil Infrastructures. In: Rizzo, P., Milazzo, A. (eds) European Workshop on Structural Health Monitoring. EWSHM 2022. *Lecture Notes in Civil Engineering*, Springer, Cham, 254: 1007–1017.

Miah, M. J., Miah, M. S., Uddin, M., Suzaudoula, M. (2018). Optimisation of mechanical properties of high performance concrete made with fly ash and blast furnace slag. In 4th International Conference on Advances in Civil Engineering (ICACE 2018), 502-507.

Miah, M. S., Werner, L. (2024). Performance Comparison of Derivative-free Optimization Methods, Proceedings of International Structural Engineering and Construction, ISEC Press, 11(2), STR-13-1- STR-13-6.

Miah, M. S. (2020). Performance Evaluation of Tall Buildings using Optimised Tuned Mass Damper. *Journal of Engineering Advancements*, 1(04), pp. 195–198.